FULL PAPER

Highly Biocompatible Carbon Nanodots for Simultaneous Bioimaging and Targeted Photodynamic Therapy In Vitro and In Vivo

Yuri Choi, Seongchan Kim, Myung-Ho Choi, Soo-Ryoon Ryoo, Jongnam Park, Dal-Hee Min,* and Byeong-Su Kim*

Photosensitizers (PSs) are light-sensitive molecules that are highly hydrophobic, which poses a challenge to their use for targeted photodynamic therapy. Hence, considerable efforts have been made to develop carriers for the delivery of PSs. Herein, a novel design is described of highly biocompatible, fluorescent, folic acid (FA)-functionalized carbon nanodots (CDs) as carriers for the PS zinc phthalocyanine (ZnPc) to achieve simultaneous biological imaging and targeted photodynamic therapy. FA is modified on PEG-passivated CDs (CD-PEG) for targeted delivery to FA-positive cancer cells, and ZnPc is loaded onto CD-PEG-FA via π–π stacking interactions. CD-PEG-FA/ZnPc exhibits excellent targeted delivery of the PS, leading to simultaneous imaging and significant targeted photodynamic therapy after irradiation in vitro and in vivo. The present CD-based targeted delivery of PSs is anticipated to offer a convenient and effective platform for enhanced photodynamic therapy to treat cancers in the near future.

1. Introduction

Biological labels that allow cellular imaging are receiving increasing attention in fluorescence microscopy, laser technology, and nanotechnology.[1] These labels are useful for tracking intracellular transport and biochemical phenomena in disease diagnosis and therapy.[2,3] Although fluorescent organic dyes and genetically engineered proteins are still widely employed as promising luminescent biological labels, semiconducting nanoparticles (quantum dots) have garnered considerable attention because of their superior physical and chemical properties such as high photoluminescence and stability, together with tunable photophysical properties.[4–6] Despite these notable advantages, the implementation of quantum dots to a broader clinical setting is still limited because of their intrinsic toxicity and the potential environmental concerns associated with the heavy metals present in the quantum dots.[7,8]

Longstanding interest in the search of benign alternatives has triggered the recent development of carbon nanoparticles (also known as C-dots, CDs) as a new class of biolabels by virtue of their biocompatibility, low toxicity, simple preparation and high stability while retaining the advantageous photophysical features of quantum dots.[9–11] CDs are generally composed of a mixed phase of sp^2- and sp^3-hybridized carbon nanostructures in the form of conjugated carbon clusters functionalized with oxygen-bearing functional groups.[12] Aside the strong fluorescence of CDs, their unique chemical structure allows the integration of active therapeutic molecules into the sp^2 carbon frame, and their surface functional groups enable further conjugation with other molecules such as biological affinity ligands. These unique characteristics make CDs ideal for simultaneous diagnosis and therapeutics (theranostics), which lead to advances in personalized medicine.[13–15]

Photodynamic therapy has been widely practiced as a promising non-invasive therapeutic modality for the treatment of cancer.[16] In photodynamic therapy, photosensitizers (PSs) are irradiated by a specific wavelength of light, which triggers the generation of reactive oxygen species from intracellular oxygen that consequently induce cell death and necrosis of proximal tissues.[17,18] However, the limited solubility and poor selectivity of PSs often pose challenges, which inevitably require a carrier system to increase their aqueous solubility and enhance cellular internalization.[19,20] A number of approaches have been proposed to incorporate PSs into carriers such as liposomes, polymeric nanoparticles, gold nanoparticles, carbon nanotubes, and graphenes.[21–27] In addition, in order to increase the local concentration of PSs in cancer cells and avoid side effects, a common strategy is a direct conjugation of carriers with targeting ligands, such as monoclonal antibodies, proteins, peptides, steroids and folic acid.[28–30] Although many of these

Y. Choi, Prof. J. Park, Prof. B.-S. Kim
Department of Chemistry and Department
of Energy Engineering
Ulsan National Institute of Science
and Technology (UNIST)
Ulsan 689–798, Korea
E-mail: bskim19@unist.ac.kr
S. Kim, M.-H. Choi, S.-R. Ryoo, Prof. D.-H. Min
Department of Chemistry
Seoul National University
Center for RNA Research
Institute for Basic Science (IBS)
Seoul 151–744, Korea
E-mail: dalheemin@snu.ac.kr

ADVANCED
FUNCTIONAL
MATERIALS
www.afm-journal.de

Materials Views
www.MaterialsViews.com
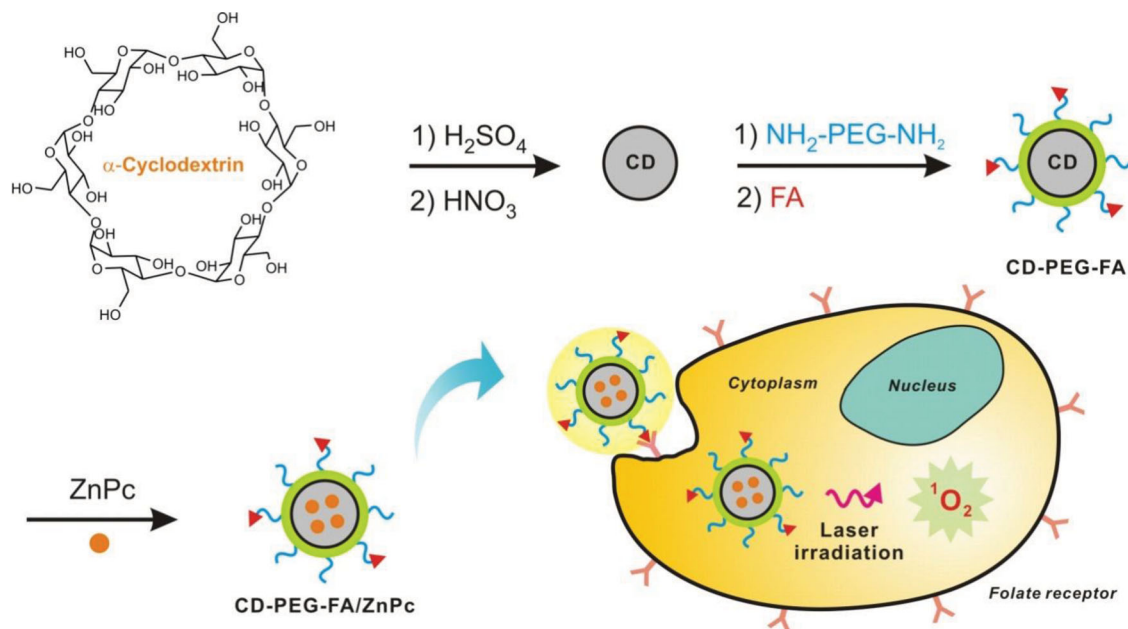
Scheme 1. Schematic illustration of the preparation of carbon nanodots (CD) from α-cyclodextrin and targeted photodynamic therapy with folic acid functionalized carbon nanodots loaded with zinc phthalocyanine (CD-PEG-FA/ZnPc).

carriers provide an effective means to increase the solubility and selectivity in aqueous media, it is still a challenging endeavor to combine in vivo therapeutic, imaging, and targeting capabilities into a single carrier.

In this work, we report a novel design of highly biocompatible, fluorescent, folic acid (FA) functionalized CD as a carrier for zinc phthalocyanine (ZnPc) PS to achieve simultaneous biological imaging and targeted photodynamic therapy (**Scheme 1**). The biocompatible and tumor-targeting FA conjugated CD is designed to selectively accumulate in tumors and to activate ZnPc upon irradiation, which enhances the selectivity and the therapeutic efficacy of photodynamic therapy both in vitro and in vivo. Specifically, the CD is synthesized via the thermal decomposition of α-cyclodextrin as a sugar-derived molecular precursor. The surface of CD is subsequently passivated with poly(ethylene glycol) diamine (PEG) to enhance its fluorescence as well as to increase the biocompatibility.[31] Surface-passivating ligands are known to play a pivotal role in increasing the fluorescence efficiency by decreasing the effective hole-trapping after generation of the exciton pair on the surface of CDs.[32] The PEG-passivated CD (CD-PEG) is further modified with FA to afford CD-PEG-FA for the targeted delivery to FA-positive cancer cells (see Supporting Information for experimental details). Owing to its high affinity for cancerous cells and stability, FA is an ideal ligand for the folate receptors that are overexpressed in various types of human cancer cells.[33] In addition, as a second-generation PS, ZnPc possesses good cytotoxic efficiency.[34]

2. Results and Discussion

The suspension of as-prepared CD was highly stable in aqueous solution, with a zeta-potential of -39.8 ± 0.45 mV.

The negative surface charge clearly indicated the presence of surface functional groups such as carboxylic acid and alcohol groups, imparting sufficient colloidal stability to the CDs. As shown in **Figure 1**a, the broad UV/vis absorption of the as-prepared CD and surface-passivated CD-PEG and CD-PEG-FA at approximately 230 nm represents the typical absorption of an aromatic system, reminiscence of an sp^2-carbon network.[35] In addition, the successful functionalization of FA onto the CD surface was clearly evident from the peak at 283 nm.[36] The zeta-potentials of CD-PEG and CD-PEG-FA were determined to be -12.4 ± 0.75 and -8.24 ± 1.96 mV (pH 7.3), respectively, suggesting the loss of the carboxylic acid groups upon surface passivation. Moreover, CD-PEG and CD-PEG-FA displayed bright blue emission under UV irradiation (inset in Figure 1a). For reference, the quantum yield (QY) of as-prepared CDs using quinine sulfate was measured to be 2.1%. After surface passivation, however, the QYs increased significantly to 7.8% for CD-PEG and 10.9% for CD-PEG-FA (Figure S1). Furthermore, the exciton lifetime was determined by the time-correlated single photon counting (TCSPC) technique, yielding 1.55, 4.13, and 5.52 ns for CD, CD-PEG, and CD-PEG-FA, respectively. This trend matches well with the QY of respective CD derivatives (Figure S2 in Supporting Information). The fluorescence emission maxima were located at 450 nm for both CD-PEG and CD-PEG-FA (λ_{ex} = 360 nm), and the broad emission peak maxima were strongly dependent on the excitation wavelength, similar to typical CDs reported (Figure 1b and Figure S3 in Supporting Information).[37,38]

FT-IR spectroscopy revealed changes in the chemical functional groups on the CDs upon surface passivation. The as-prepared CDs showed peaks at 1068 (C–O stretching), 1608 (C=C stretching), 2848 and 2925 cm^{-1} (C–H stretching), and a broad peak at 3457 cm^{-1} that corresponded to carboxylic acid and hydroxyl groups (Figure 1c). Upon surface passivation, the

Materials
Views
www.MaterialsViews.com

ADVANCED
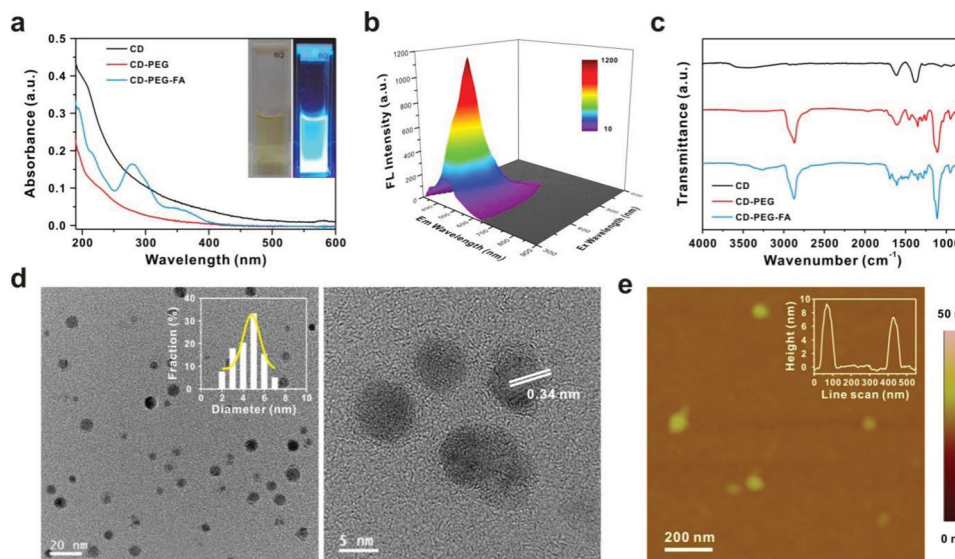FUNCTIONAL
MATERIALS
www.afm-journal.de

FULL PAPER

Figure 1. (a) UV-vis absorbance spectra of CD, CD-PEG, and CD-PEG-FA. Inset shows the CD-PEG-FA suspension (left) under room light and (right) UV illumination at 365 nm. (b) Three-dimensional fluorescence spectra of CD-PEG-FA under varying excitation wavelengths from 300 to 600 nm with 10-nm increments. (c) FT-IR spectra of CD, CD-PEG, and CD-PEG-FA. (d) TEM images of CD-PEG-FA with a corresponding size distribution histogram. (e) Representative height-mode AFM topography image of CD-PEG-FA with a line scan profile in the inset.

presence of new bands at 1594 (N-H in-plane) and 1340 cm^{-1} (C–N stretching) confirmed the successful formation of amide groups by chemical conjugation of the surface carboxylic acid groups of the CDs with the amine-terminated PEG. Furthermore, the PEG surface passivation significantly increased the peak due to the C–O groups at 1102 cm^{-1}. After passivation with FA, CD-PEG-FA exhibited characteristic peaks at 1481, 1605, and 1697 cm^{-1} which corresponded to FA.[39] In accordance with the above results, high-resolution X-ray photoelectron spectroscopy (XPS) measurements further confirmed the composition of the respective CDs and the successful surface passivation (Figure S4 and Table S1 in Supporting Information).

The size and morphology of the CDs were observed by transmission electron microscopy (TEM) and atomic force microscopy (AFM). The TEM images showed a spherical morphology of the CDs, with an average diameter of 4.5 ± 0.2 nm for CD-PEG-FA (Figure 1d). The interlayer spacing of 0.34 nm, observed using high-resolution TEM, corresponded to that of graphitic carbon, representing the graphitic nature of the CDs. The AFM line scans indicated that the diameters of CD, CD-PEG and CD-PEG-FA were approximately 3.5, 4.4, and 4.9 nm, respectively, consistent with the stepwise surface functionalization with PEG and FA of the CDs (Figure 1e and Figure S5 in Supporting Information).

After characterization of the chemically functionalized CDs, ZnPc was loaded onto CD-PEG-FA by π–π stacking interactions. The CD-PEG-FA carrying ZnPc (CD-PEG-FA/ZnPc) exhibited red-shifted absorption peaks at 607 and 689 nm, which originated from ZnPc and strongly quenched the fluorescence of ZnPc, suggesting the successful loading of ZnPc (Figure S6 in Supporting Information).[25,40–43] The characteristic fluorescence spectrum and QY of CD-PEG-FA did not alter upon loading with ZnPc (6 wt% of ZnPc/CD-PEG-FA, Figure S3 in Supporting Information). AFM and dynamic light scattering (DLS) analysis showed no aggregation of CD-PEG-FA/ZnPc,

suggesting the uniform loading of ZnPc onto the surface of CD-PEG-FA carrier by π–π stacking interactions (Figure S7 in Supporting Information).

To investigate the efficacy of the CD-PEG-FA/ZnPc in targeted delivery and photodynamic therapy, we employed human cervical cancer HeLa cells, which are known to overexpress the folate receptor-α.[44] Initially, a conventional CCK-8 based cell viability assay suggested the superior biocompatibility of CD and its derivatives toward the HeLa cells under the present working concentration ranges of the respective CD derivatives (5–450 μg/mL), as reported in other work (Figure S8 and S9 in Supporting Information).[45] As shown in **Figure 2** and Figure S10 in Supporting Information, the targeting of CD-PEG, CD-PEG-FA, and CD-PEG-FA/ZnPc was evaluated after incubation with the HeLa cells for 12 h, by monitoring the blue and red fluorescence of CD ($\lambda_{ex}/\lambda_{em}$ = 358/461 nm) and ZnPc ($\lambda_{ex}/\lambda_{em}$ = 647/665 nm), respectively, to probe the internalization of CD and ZnPc under a fluorescence microscope. As expected, the cells incubated with CD-PEG-FA displayed intense CD fluorescence in the cytoplasm, whereas CD-PEG exhibited no sign of internalization into the HeLa cells, even when treated with an identical concentration of CD-PEG-FA. In accord with CD-PEG-FA, CD-PEG-FA/ZnPc was also internalized in the HeLa cells, with prominent fluorescence signals of both the blue (CD) and red (ZnPc) channels, indicating the successful intracellular delivery of ZnPc by the CD carrier. To clarify the targeting role of FA, a competition assay was performed with free FA. The folate receptors on the HeLa cells were first saturated with free FA, followed by the introduction of CD-PEG-FA/ZnPc, which clearly demonstrated no cellular internalization (Figure 2d). The targeting affinity and efficacy based on the FA and folate receptor was further evaluated using folate receptor overexpressed (FR+) and folate receptor deficient (FR-) cell lines. After incubated with CD-PEG/ZnPc and CD-PEG-FA/ZnPc, FR+ MDA-MB-231 cells were monitored by flu-
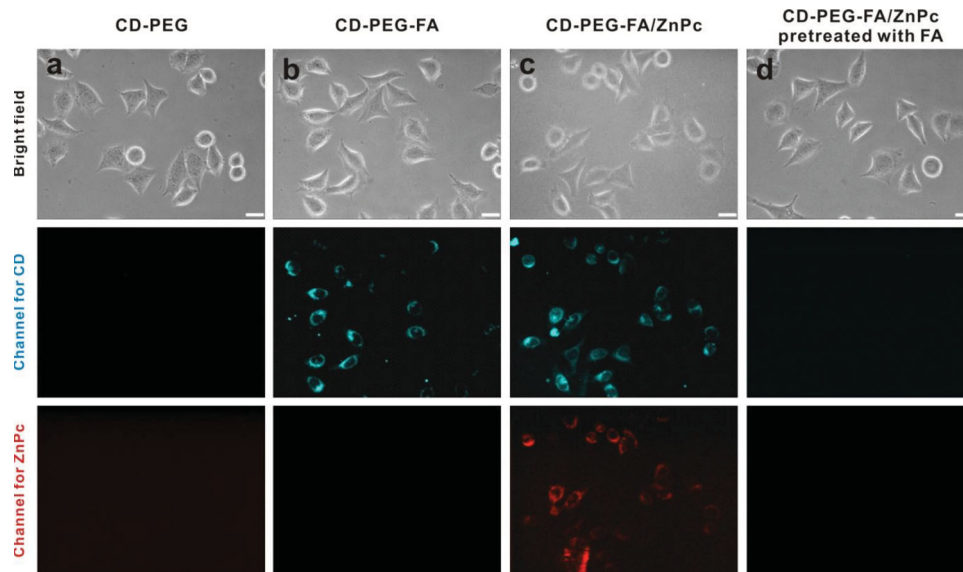
Figure 2. (a–d) Bright-field and fluorescence images of HeLa cells treated with CD derivatives (50 μg/mL) for 12 h. (a) CD-PEG, (b) CD-PEG-FA, (c) CD-PEG-FA/ZnPc and (d) CD-PEG-FA/ZnPc pretreated with folic acid. Fluorescence signals of (blue) CDs and (red) ZnPc were observed at 461 nm (λ_{ex} = 358 nm) and 665 nm (λ_{ex} = 647 nm), respectively. Scale bar is 20 μm.

orescence microscope, and FR-A549 cells were used as a negative control. Figure S11 showed that the fluorescent CD and ZnPc were localized with intracellular cytoplasm, indicating that CD-PEG-FA/ZnPc was effectively internalized into the cells through the close rapport between FA and FR. However, no significant fluorescence was observed in FR-A549 cells and even CD-PEG/ZnPc treated MDA-MB-231 cells.

Taken together, these results corroborate that the folate receptors overexpressed on the surface of the HeLa cells facilitate the recognition of the CD-PEG-FA and induce the preferential uptake of CD-PEG-FA by receptor-mediated endocytosis.[44,46,47] Since the passive targeting of the PS is inadequate for in vivo photodynamic treatment through systemic administration, the modification of active targeting ligands to the surface of the CD is critical to increase the local concentration of the PS in tumors, and thus helps in avoiding side effects and maximizes the therapeutic efficacy.

Next, we performed a photodynamic therapy on the HeLa cells with the CD derivatives (**Figure 3**). The cells were exposed to the CD derivatives for 12 h followed by laser irradiation (660 nm, 30 mW/cm^2) for 10 min. Significant cell death was observed in CD-PEG-FA/ZnPc, whereas other samples treated with CD-PEG, CD-PEG-FA and FA-pretreated CD-PEG-FA/ZnPc did not exhibit measurable photodynamic activity (Figure 3 and Figure S12 in Supporting Information). In addition, the generation of the active singlet oxygen species via photoinduced energy transfer from ZnPc was quantified by using the singlet oxygen sensor green (SOSG) reagent;[48,49] the green fluorescence (λ_{em} = 525 nm) is known to increase when SOSG reacts with singlet oxygen generated from the PS, which can be used for quantification of singlet oxygen generation.[50,51] Figure 3e shows the fluorescence intensity as a function of irradiation time; the intensity gradually increases upon irradiation with an LED (30 mW/cm^2). While the control ZnPc without SOSG did not exhibit any fluorescence changes, ZnPc and

CD-PEG-FA/ZnPc mixed with SOSG showed an increase in the fluorescence intensity upon irradiation. It is of note that SOSG alone showed increasing fluorescence intensity upon irradiation, since SOSG itself can act as a PS and thus generate singlet oxygen species.[52] Because of intermolecular energy transfer between ZnPc and CD, the CD-PEG-FA/ZnPc did not effectively generate singlet oxygen relative to free ZnPc with SOSG. However, singlet oxygen generation was considerably accelerated upon the addition of cell lysate (Figure 3e, t = 25 min), indicating the release of ZnPc from CD via the competitive displacement of ZnPc by interaction with the biomolecules in cell lysate, thus enhancing the therapeutic efficiency of photodynamic therapy.

Quantitative CCK-8 cell viability assays, used to investigate the effects of concentration and laser irradiation, were carried out using the HeLa cells incubated for 12 h. For example, the cell viabilities of free ZnPc, CD-PEG-FA/ZnPc without irradiation, and CD-PEG-FA/ZnPc with irradiation were determined to be 60.9%, 94.2%, and 8.2%, respectively, at a concentration of 100 μg/mL. The result clearly confirms that the generation of singlet oxygen, and thus, effective photodynamic action necessitates both suitable concentrations of the PS and appropriate light irradiation. Moreover, the significant difference in the viability between the irradiated CD-PEG-FA/ZnPc and free ZnPc is consistent with the preferential internalization of CD-PEG-FA/ZnPc into the HeLa cells, which results in considerably improved therapeutic efficacy of photodynamic action.

Encouraged by the high PDT efficacy in vitro, we next investigated the PDT efficacy of the CD-mediated PS delivery system in animal models. Tumor-bearing mice were first prepared by subcutaneously injecting a suspension of the HeLa cells (6×10^6 cells) in sterilized 1X PBS solution into BALB/c nude mice (6 weeks old). To monitor the biodistribution of the CD derivatives in vivo, the fluorescence images from the whole body were obtained at designated time points after the various CD deriva-
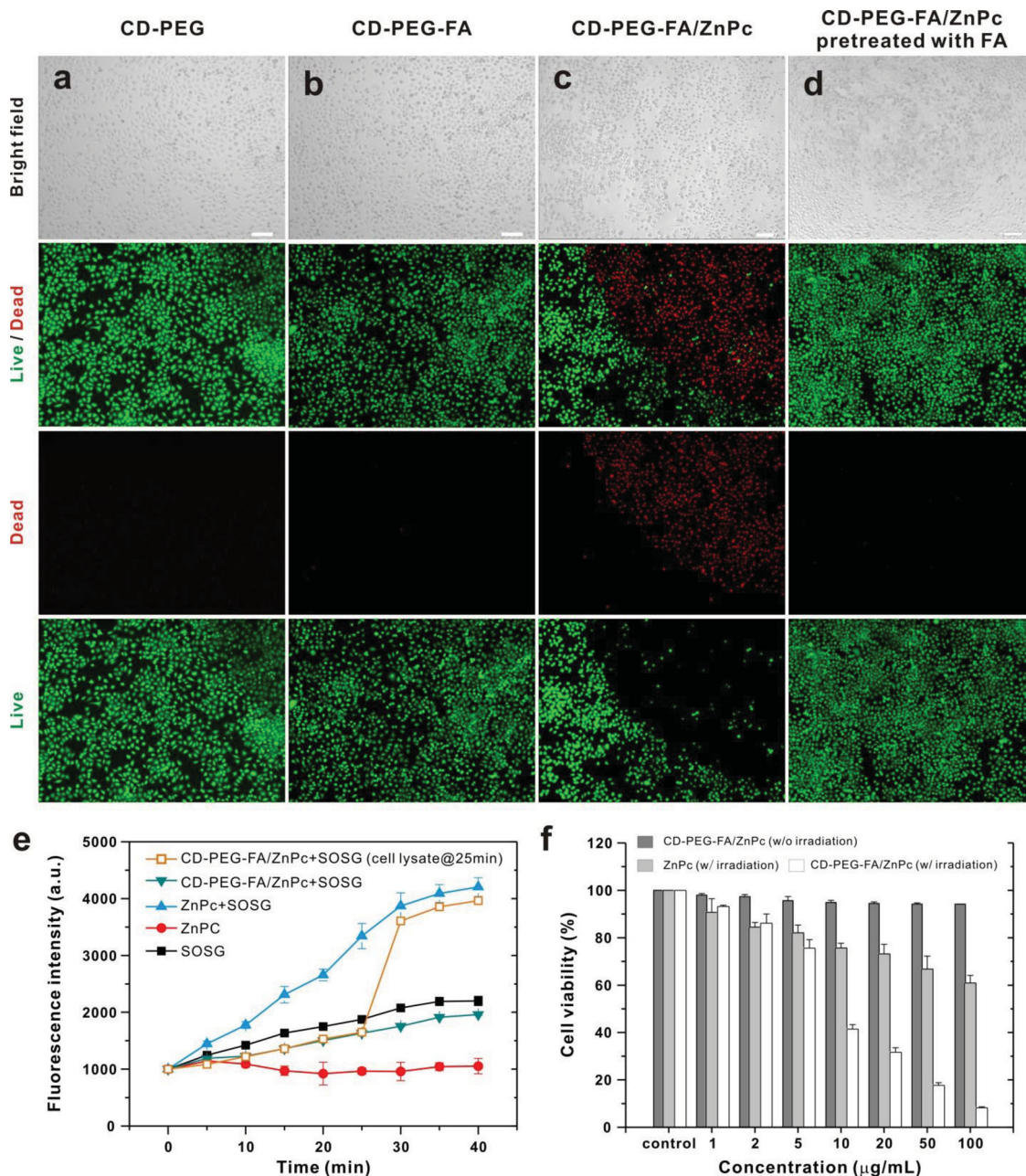
www.MaterialsViews.com

ADVANCED
FUNCTIONAL
MATERIALS
www.afm-journal.de

FULL PAPER

Figure 3. (a–d) (top panel) Bright-field and fluorescence images of HeLa cells treated with CD derivatives (50 µg/ml) for 12 h, followed by irradiation for 10 min with a 660 nm laser (30 mW/cm^2), and (bottom panels) live and dead cells colored green and red, respectively, by live/dead assay. (a) CD-PEG, (b) CD-PEG-FA, (c) CD-PEG-FA/ZnPc, and (d) CD-PEG-FA/ZnPc with pretreatment of excess free FA. Scale bar is 100 µm. (e, f) Quantitative evaluation of photodynamic effect. (e) Singlet oxygen detection test using a singlet oxygen sensor green (SOSG) reagent. Time-dependent fluorescent intensity ($\lambda_{ex}/\lambda_{em} = 504/530$ nm) with irradiation by using a 660 nm laser (30 mW/cm^2). Concentrations of ZnPc and SOSG used are 3.8 and 2.5 µM, respectively. Note that the addition of cell lysate (1 µL) in CD-PEG-FA/ZnPc did not change the effective concentrations of ZnPc and SOSG. (f) Cell viability assay depending on the concentration of ZnPc loaded CD-PEG-FA and ZnPc with and without irradiation for 10 min. All experiments were carried out in triplicate; the error bars represent the standard deviation.

tives were injected into tail veins. As shown in **Figure 4**a and b, the mice treated with CD-PEG-FA/ZnPc showed strong fluorescence signals corresponding to ZnPc in tumors, with gradual increase in the fluorescence intensity over time, in contrast to the mice treated with CD-PEG/ZnPc or CD-PEG-FA. Biodistribution of the CD derivatives was further examined by imaging major organs that were excised after sacrificing the mice

administered with the CD derivatives. Fluorescence images of the major organs in Figure 4c showed that the fluorescence corresponding ZnPc were intense in liver and spleen rather than tumor in case of the mouse injected with CD-PEG/ZnPc, suggesting that most of the CDs omitting targeting ligand FA leaked out by circulation and prominently accumulated in reticuloendothelial system of the liver and spleen.[53,54] These results
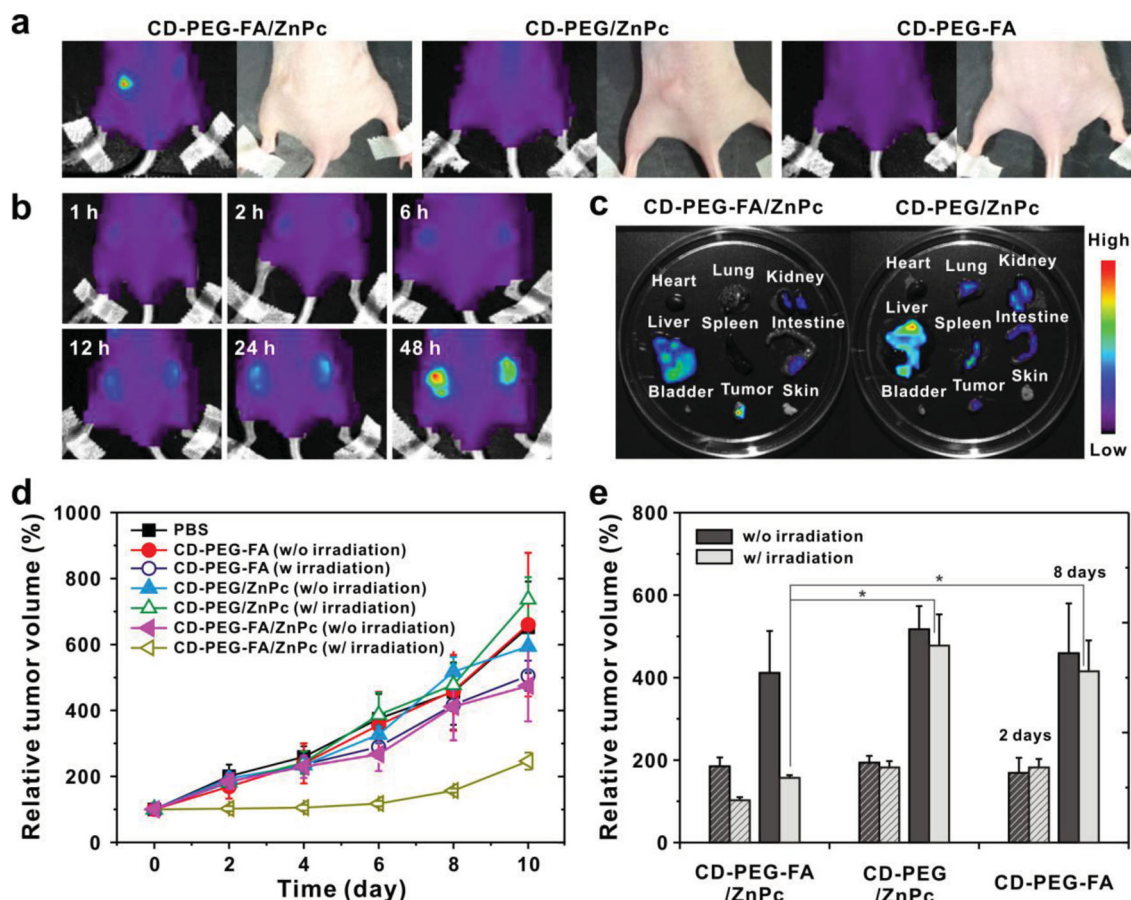
ADVANCED
FUNCTIONAL
MATERIALS
www.afm-journal.de

Materials
Views
www.MaterialsViews.com

FULL PAPER

Figure 4. (a) Fluorescence of ZnPc (excited at 660 nm) in tumor was imaged after 12 h injection of CD-PEG-FA/ZnPc, CD-PEG/ZnPc, and CD-PEG-FA (0.5 mg of ZnPc/kg mouse). (b) CD-PEG-FA/ZnPc suspensions were injected into tail veins of tumor-bearing mice and the fluorescent signals were obtained at various time points (1, 2, 6, 12, 24, and 48 h). (c) Ex vivo fluorescence images of major organs of mice. The fluorescent signals corresponding to ZnPc (excited at 660 nm) from major organs, tumor, and skin were obtained after 12 h of i.v. injection of CD-PEG-FA/ZnPc and CD-PEG/ZnPc into tumor-bearing mice. FA-conjugated CD delivered and released ZnPc to tumor effectively, in contrast with the CD lacking FA. (d,e) Relative tumor volumes measured over time after the tumor-bearing mice were treated with various CD derivatives. Tumor-bearing mice were separated into 6 groups: (i) PBS control; (ii) CD-PEG-FA without irradiation; (iii) CD-PEG-FA with irradiation; (iv) CD-PEG/ZnPc without irradiation; (v) CD-PEG/ZnPc with irradiation; (vi) CD-PEG-FA/ZnPc without irradiation; (vii) CD-PEG-FA/ZnPc with irradiation ($n = 4$ for each group). Irradiation was performed using a 660-nm laser at 0.3 W/cm^2. Tumor volumes were measured over 10 days. It is notable that no significant increase in tumor volume was observed for 8 days in mice treated with CD-PEG-FA/ZnPc with irradiation. P values were calculated by Student's t-test: * for $p < 0.05$, $n = 4$.

showed that conjugation of FA to CD played an important role in greatly improving the active tumor-targeting capability of the ZnPc delivery vehicle to folate receptor-overexpressing tumors.

Finally, to investigate the therapeutic efficacy in vivo, changes in tumor volumes were monitored for 10 days after CD-PEG-FA, CD-PEG/ZnPc, and CD-PEG-FA/ZnPc (0.5 mg of ZnPc/kg of mouse) were intravenously injected to mice whose tumor volumes were ~70 mm^3. The same volume of saline was treated as a control, and the relative tumor volumes were determined by comparing its volumes at different time points to the initial volumes (Figures 4d and e). After irradiation with a 660-nm laser (0.3 W/cm^2, 20 min), the mice treated with CD-PEG-FA/ZnPc showed remarkable suppression of tumor growth as compared to the control mice for 8 days. However, the mice treated with CD-PEG/ZnPc and CD-PEG-FA, with or without laser irradiation, showed no notable difference in tumor size compared to the controls. This result was in agreement with the in vitro data, indicating that a combination of targeted delivery

of ZnPc and light irradiation can effectively induce cancer cell death in vivo. Collectively, the in vivo study suggested that the present tumor-targeted CD-based PDT therapeutic agent delivery system can effectively induce the accumulation of the PS-loaded CDs in tumors, thus leading to enhanced therapeutic efficacy with a relatively small quantity of ZnPc.

3. Conclusion

We have developed a novel theranostic platform based on FA-conjugated CD loaded with ZnPc in the present study. We have successfully demonstrated the targeted delivery of a PS via FA-mediated endocytosis of biocompatible CD-PEG-FA/ZnPc and therapeutic photodynamic efficacy by singlet oxygen generation from the internalized ZnPc upon light irradiation in vitro and in vivo. We anticipate that the present CD-based targeted delivery of the PS would offer a convenient and effective

platform for enhanced photodynamic therapy to treat cancers in the near future because of its excellent biocompatibility, bioimaging and targeting capability, and therapeutic efficacy.

4. Experimental Section

Materials: α-Cyclodextrin, poly(ethylene glycol) diamine (M_w = 1500 g/mol), folic acid, and zinc phthalocyanine (ZnPc) were purchased from Sigma-Aldrich. H_2SO_4, HNO_3, and K_2CO_3 were purchased from Daejung Chemical (Korea). Cell counting kit-8 (CCK-8) was purchased from Dojindo Laboratories (Japan). Live/dead viability/cytotoxicity kit and singlet oxygen sensor green (SOSG) reagent were purchased from Molecular Probes (USA). 10X PBS phosphate buffered saline (PBS), Dulbecco's Modified Eagle's Medium (DMEM), and fetal bovine serum (FBS) were purchased from WELGENE (Korea).

Preparation of CDs: CDs were synthesized by dehydrating carbohydrates using concentrated sulfuric acid. In this case, 2.00 g of α-cyclodextrin was slowly added to 8 mL of H_2SO_4, to which 5 mL of water was added to dissolve the α-cyclodextrin. The black solution was stirred vigorously for 1 h and then diluted with 40 mL of water. The solution was then centrifuged at 4000 rpm for 10 min, and the supernatant was discarded. The precipitate was washed twice with distilled water, re-suspended in 5 mL of water and 6 mL of HNO_3 (22.5 mM), and sonicated for 1 h. The resulting solution was refluxed under nitrogen for 12 h at 120 °C and then neutralized with K_2CO_3. After excess K_2CO_3 was removed, the CDs were subjected to extensive dialysis (SpectraPore MWCO 1000) for 1 day to remove excess salts.

Surface Passivation of CDs: To passivate the CDs, the solutions were diluted one to ten parts with distilled water and refluxed for 72 h at 120 °C with poly(ethylene glycol) diamine (PEG, 150 mM). After the reflux, each of the samples was subjected to extensive dialysis against water for 2 days. To prepare the FA-conjugated CD-PEG, FA (10 mM) and 1-ethyl-3-(3-dimethylaminopropyl)carbodiimide (EDC, 10 mM) were mixed in 1.0 mL of distilled water saturated with $NaHCO_3$, followed by incubation with CD-PEG (1.0 mg/mL) at room temperature for 18 h. The amount of conjugated FA in CD-PEG-FA, as estimated by measuring the UV/Vis absorbance, was 5.8 mg/mL-CD-PEG-FA. Then, the mixture was subjected to extensive dialysis against distilled water for purification for 2 days. For ZnPc loading to CD-PEG-FA, an ethanolic solution of ZnPc (2.0 mg) was subjected to solvent evaporation prior to mixing with CD-PEG-FA (1.0 mg/mL). Then, the mixture was sonicated for 1 h on an ice bath and filtered through polyvinylidene difluoride (PVDF) syringe filters (0.2 μm). The loading capacity of ZnPc to CD-PEG-FA, calculated from the standard curve of the UV-vis absorbance of ZnPc, was about 60 μg of ZnPc per milligram of CD-PEG-FA.

Fluorescence Quenching Test: To estimate the ZnPc loading to CD-PEG-FA, the fluorescence emission spectra of ZnPc (0.4 μM) were obtained at an excitation wavelength of 650 nm with or without CD-PEG-FA (1.0 mg/ml) by using a fluorometer (BioTek, U.S.A.).

Cell Culture: HeLa cell lines and MDA-MD-231 cell lines were grown in DMEM containing 4.5 g/L D-glucose containing 10% FBS, 1% penicillin, and streptomycin, under an atmosphere of 5% CO_2 and at 37 °C. A549 cell lines were grown in RPMI 1640 with same components and conditions.

Cellular Toxicity Test: To investigate the cytotoxicity of the CDs, we carried out the CCK-8 cell viability assay. HeLa cells (1×10^4 cells/well) were seeded in a 96-well plate for 24 h, and CDs were treated with the HeLa cells at varying concentrations (0–450 μg/mL) in serum-containing media. After 12 h incubation, the cells were carefully washed with 1× PBS; then, CCK-8 assay solution with serum-free media was added, incubation was carried out for 1 h, and the absorbance at 450 and 670 nm was measured by using a microplate reader (Molecular Devices, Inc., USA). To investigate the quantitative cell viability related to the photodynamic effect of CD-PEG-FA/ZnPc, HeLa cells (1×10^4 cells/well) were plated in a 96-well plate, incubated for 24 h, and incubated with various concentrations of CD-PEG-FA/ZnPc. After 12 h incubation,

each well was irradiated with a 660-nm LED laser (Mikwang Electronics, 30 mW/cm²) for 10 min, and then, the medium was replaced with a serum-containing medium. After further incubation for 12 h, the CCK-8 cell viability assay was performed as described above. All experiments were carried out in triplicate.

Cellular Imaging: HeLa cells (1.2×10^5 cells/well) were seeded in a 4-well glass plate. After 24 h incubation, CDs derivatives were added to each well in a serum-free medium for 12 h. To confirm the effect of folate receptor-mediated cell uptake, free FA was excessively treated for 2 h prior to treating FA-conjugated CD derivatives. After 12 h incubation, the cells were carefully rinsed with 1× PBS, and the medium was replaced with a serum-containing medium. MDA-MB-231 cells and A549 cells were also prepared with same procedure excluding free FA treat. Cell images were obtained using a Ti inverted fluorescence microscope with a 10× (1.4 numerical aperture) objective (Olympus, Japan), a Deltavision high-resolution microscope, and In-cell analyzer 2000 (GE Healthcare, Korea). To investigate the photodynamic effect, CD-PEG-FA/ZnPc (50 μg/mL) with a serum-free medium was treated with HeLa cells (1.2×10^5 cells/well), which had been preincubated in a 12-well plate for 24 h. After the medium exchange to a serum-containing medium, the cells were irradiated with a 660-nm fiber-coupled laser (LaserLab, Korea, 30 mW/cm²) for 10 min. After further 4 h incubation, each well was treated with Live/Dead assay reagent, based on the manufacturer's protocol. Then, fluorescence images of the cells were obtained by using a Ti inverted fluorescence microscope with a 10× objective.

Singlet Oxygen Detection: The SOSG reagent is highly selective to singlet oxygen (SO), and it emits strong green fluorescence in the presence of SO at 530 nm (λ_{ex} = 504 nm). SOSG (2.5 μM) dissolved in 2% methanol was added to ZnPc (3.8 μM) and CD-PEG-FA/ZnPc (1.0 mg/mL), and then, the generation of SO was induced by irradiation using a 660-nm LED (30 mW/cm²). After time-dependent irradiation, green fluorescence emission from the samples was observed at 530 nm by using a fluorometer (BioTek, USA).

Characterization: UV/vis spectrophotometer (UV-2550, Shimadzu) was used to record the absorbance for concentration control and comparison. Absorbance curves were compared to ascertain the similarity in concentration, after which the samples were adjusted for comparison. Fluorescence data were obtained by using a fluorometer (Agilent). Three-dimensional fluorescence spectrum of the CDs was obtained with an FP-8300 spectrofluorometer (JASCO). Transmission electron microscopy (TEM, JEM-2100, JEOL) and atomic force microscopy (AFM, Dimension 3100, Veeco) analyses were performed to investigate the size and morphology of the CDs. To confirm the functional groups after passivation, XPS (K-alpha, Thermo Fisher) and FT-IR (Agilent) analyses were performed.

Photoluminescence Lifetime Measurement: The exciton lifetime was determined by the time-correlated single photon counting (TCSPC) technique. A computer-controlled diode laser with 375 nm wavelength, 54 ps pulse width, and 40 MHz repetition rate was used as an excitation source. The PL emission was spectrally resolved by using some collection optics and a monochromator (PicoQuant). The TCSPC module (PicoHarp 300E, PicoQuant) with a MCP-PMT (R3809U-5x series, Hamamatsu) was used for ultrafast detection. The total instrument response function (IRF) for PL decay was less than 30 ps, and the temporal time resolution was less than 10 ps. Deconvolution of the actual fluorescence decay and IRF was performed by using a fitting software (FlouFit, PicoQuant) to deduce the time constant associated with each exponential decay.

In vivo Targeting and Biodistribution Study: Male BALB/c-nude mice (6 weeks old) were purchased from Japan SLC, Inc. (Shizuoka, Japan). All animal experiments were carried out in compliance with the Institutional Animal Care and Use Committees (IACUC) of Seoul National University. Tumor-bearing mice were prepared by subcutaneously injecting a suspension of the Hela cells (6×10^6 cells) in sterilized 1× PBS (n = 4). When the tumor size reached ~70 mm³, CD-PEG-FA/ZnPc, CD-PEG/ZnPc, and CD-PEG-FA in 1× PBS solution (0.5 mg ZnPc/kg) were injected into the tail veins of the tumor-bearing mice. As a control, one group of mice was treated with the same volume of 1× PBS. Fluorescent

signals from the mice were obtained by using an optical molecular imaging system, Optix MX3 (GE Healthcare, Korea), at various time points. To examine the biodistribution of the injected ZnPc, major organs (heart, lung, liver, etc.) were collected into a petri-dish after 12 h injection and imaged.

In vivo Photodynamic Therapy: Tumor-bearing mice were first prepared in four groups ($n = 4$). When the tumor size reached ~70 mm^3, the mice were treated with CD-PEG-FA/ZnPc, CD-PEG/ZnPc, and CD-PEG-FA in 1X PBS (0.5 mg ZnPc/kg) by intravenous injection. As a control, a group of mice was treated with the same volume of saline. The mice were segregated into 6 groups: (1) saline; (2) CD-PEG-FA without irradiation; (3) CD-PEG-FA with irradiation; (4) CD-PEG/ZnPc without irradiation; (5) CD-PEG/ZnPc with irradiation; (6) CD-PEG-FA/ZnPc without irradiation; (7) CD-PEG-FA/ZnPc with irradiation. For the irradiated groups, 660-nm laser (0.3 W/cm^2, 20 min) was used after 12 h of injection. The photodynamic therapeutic effects were investigated by monitoring the change in tumor volumes and body weight in each group every day up to 10 days. The tumor volumes were calculated by using the equation of length $\times$ (width)$^2 \times 1/2$, where the length and width are the longest and shortest diameters (mm) of the tumor, respectively. The relative tumor volumes were calculated relative to the initial volumes.

Statistical Analysis: All data shown mean corrected values $\pm$ SD of at least three independent experiments. Significant differences were determined based on the Student's t-test where differences were considered significant ($p < 0.05$). Statistical analyses were performed with the GraphPad Software.

Supporting Information

Supporting Information is available from the Wiley Online Library or from the author.

Acknowledgements

[1] R. Weissleder, *Nat. Rev. Cancer* **2002**, *2*, 11.
[2] J. K. Willmann, N. van Bruggen, L. M. Dinkelborg, S. S. Gambhir, *Nat. Rev. Drug Discovery* **2008**, *7*, 591.
[3] J. A. Barreto, W. O'Malley, M. Kubeil, B. Graham, H. Stephan, L. Spiccia, *Adv. Mater.* **2011**, *23*, H18.
[4] A. P. Alivisatos, *Science* **1996**, *271*, 933.
[5] X. Michalet, F. F. Pinaud, L. A. Bentolila, J. M. Tsay, S. Doose, J. J. Li, G. Sundaresan, A. M. Wu, S. S. Gambhir, S. Weiss, *Science* **2005**, *307*, 538.
[6] I. L. Medintz, H. T. Uyeda, E. R. Goldman, H. Mattoussi, *Nat. Mater.* **2005**, *4*, 435.
[7] A. M. Derfus, W. C. W. Chan, S. N. Bhatia, *Nano Lett.* **2004**, *4*, 11.
[8] R. Hardman, *Environ. Health Perspect.* **2006**, *114*, 165.
[9] S. T. Yang, L. Cao, P. G. J. Luo, F. S. Lu, X. Wang, H. F. Wang, M. J. Meziani, Y. F. Liu, G. Qi, Y. P. Sun, *J. Am. Chem. Soc.* **2009**, *131*, 11308.
[10] S. N. Baker, G. A. Baker, *Angew. Chem. Int. Ed.* **2010**, *49*, 6726.
[11] H. T. Li, Z. H. Kang, Y. Liu, S. T. Lee, *J. Mater. Chem.* **2012**, *22*, 24230.
[12] S. C. Ray, A. Saha, N. R. Jana, R. Sarkar, *J. Phys. Chem. C* **2009**, *113*, 18546.
[13] P. Huang, J. Lin, X. S. Wang, Z. Wang, C. L. Zhang, M. He, K. Wang, F. Chen, Z. M. Li, G. X. Shen, D. X. Cui, X. Y. Chen, *Adv. Mater.* **2012**, *24*, 5104.
[14] J. Tang, B. Kong, H. Wu, M. Xu, Y. C. Wang, Y. L. Wang, D. Y. Zhao, G. F. Zheng, *Adv. Mater.* **2013**, *25*, 6569.
[15] Q. L. Wang, X. X. Huang, Y. J. Long, X. L. Wang, H. J. Zhang, R. Zhu, L. P. Liang, P. Teng, H. Z. Zheng, *Carbon* **2013**, *59*, 192.
[16] D. E. J. G. J. Dolmans, D. Fukumura, R. K. Jain, *Nat. Rev. Cancer* **2003**, *3*, 380.
[17] B. W. Henderson, T. J. Dougherty, *Photochem. Photobiol.* **1992**, *55*, 145.
[18] J. F. Lovell, T. W. B. Liu, J. Chen, G. Zheng, *Chem. Rev.* **2010**, *110*, 2839.
[19] Y. N. Konan, R. Gurny, E. Allemann, *J. Photochem. Photobiol. B* **2002**, *66*, 89.
[20] D. Bechet, P. Couleaud, C. Frochot, M. L. Viriot, F. Guillemin, M. Barberi-Heyob, *Trends Biotechnol.* **2008**, *26*, 612.
[21] A. S. L. Derycke, P. A. M. de Witte, *Adv. Drug Delivery Rev.* **2004**, *56*, 17.
[22] K. J. Son, H. J. Yoon, J. H. Kim, W. D. Jang, Y. Lee, W. G. Koh, *Angew. Chem. Int. Ed.* **2011**, *50*, 11968.
[23] W. S. Kuo, C. N. Chang, Y. T. Chang, M. H. Yang, Y. H. Chien, S. J. Chen, C. S. Yeh, *Angew. Chem. Int. Ed.* **2010**, *49*, 2711.
[24] G. Obaid, I. Chambrier, M. J. Cook, D. A. Russell, *Angew. Chem. Int. Ed.* **2012**, *51*, 6158.
[25] B. Tian, C. Wang, S. Zhang, L. Z. Feng, Z. Liu, *ACS Nano* **2011**, *5*, 7000.
[26] F. Li, S. Park, D. Ling, W. Park, J. Y. Han, K. Na, K. Char, *J. Mater. Chem. B* **2013**, *1*, 1678.
[27] Z. Zhu, Z. W. Tang, J. A. Phillips, R. H. Yang, H. Wang, W. H. Tan, *J. Am. Chem. Soc.* **2008**, *130*, 10856.
[28] W. M. Sharman, J. E. van Lier, C. M. Allen, *Adv. Drug Delivery Rev.* **2004**, *56*, 53.
[29] S. Verma, G. M. Watt, Z. Mal, T. Hasan, *Photochem. Photobiol.* **2007**, *83*, 996.
[30] F. Schmitt, L. Juillerat-Jeanneret, *Anti-Cancer Agents Med. Chem.* **2012**, *12*, 500.
[31] H. Choi, S. J. Ko, Y. Choi, P. Joo, T. Kim, B. R. Lee, J. W. Jung, H. J. Choi, M. Cha, J. R. Jeong, I. W. Hwang, M. H. Song, B. S. Kim, J. Y. Kim, *Nat. Photonics* **2013**, *7*, 732.
[32] Y. P. Sun, B. Zhou, Y. Lin, W. Wang, K. A. S. Fernando, P. Pathak, M. J. Meziani, B. A. Harruff, X. Wang, H. F. Wang, P. J. G. Luo, H. Yang, M. E. Kose, B. L. Chen, L. M. Veca, S. Y. Xie, *J. Am. Chem. Soc.* **2006**, *128*, 7756.
[33] C. P. Leamon, P. S. Low, *Drug Disc. Today* **2001**, *6*, 44.
[34] J. W. Owens, R. Smith, R. Robinson, M. Robins, *Inorg. Chim. Acta* **1998**, *279*, 226.
[35] L. B. Tang, R. B. Ji, X. K. Cao, J. Y. Lin, H. X. Jiang, X. M. Li, K. S. Teng, C. M. Luk, S. J. Zeng, J. H. Hao, S. P. Lau, *ACS Nano* **2012**, *6*, 5102.
[36] Y. C. Song, W. Shi, W. Chen, X. H. Li, H. M. Ma, *J. Mater. Chem.* **2012**, *22*, 12568.
[37] S. N. Qu, X. Y. Wang, Q. P. Lu, X. Y. Liu, L. J. Wang, *Angew. Chem. Int. Ed.* **2012**, *51*, 12215.
[38] S. J. Zhu, Q. N. Meng, L. Wang, J. H. Zhang, Y. B. Song, H. Jin, K. Zhang, H. C. Sun, H. Y. Wang, B. Yang, *Angew. Chem. Int. Ed.* **2013**, *52*, 3953.
[39] H. Huang, Q. Yuan, J. S. Shah, R. D. K. Misra, *Adv. Drug Delivery Rev.* **2011**, *63*, 1332.

FULL PAPER

[40] M. Zhang, T. Murakami, K. Ajima, K. Tsuchida, A. S. D. Sandanayaka, O. Ito, S. Iijima, M. Yudasaka, *Proc. Natl. Acad. Sci. USA* **2008**, *105*, 14773.

[41] X. M. Sun, Z. Liu, K. Welsher, J. T. Robinson, A. Goodwin, S. Zaric, H. J. Dai, *Nano Res.* **2008**, *1*, 203.

[42] Z. Liu, J. T. Robinson, X. M. Sun, H. J. Dai, *J. Am. Chem. Soc.* **2008**, *130*, 10876.

[43] N. Karousis, J. Ortiz, K. Ohkubo, T. Hasobe, S. Fukuzumi, A. Sastre-Santos, N. Tagmatarchis, *J. Phys. Chem. C* **2012**, *116*, 20564.

[44] L. S. Wang, L. C. Wu, S. Y. Lu, L. L. Chang, I. T. Teng, C. M. Yang, J. A. A. Ho, *ACS Nano* **2010**, *4*, 4371.

[45] H. Q. Tao, K. Yang, Z. Ma, J. M. Wan, Y. J. Zhang, Z. H. Kang, Z. Liu, *Small* **2012**, *8*, 281.

[46] C. P. Leamon, J. A. Reddy, *Adv. Drug Delivery Rev.* **2004**, *56*, 1127.

[47] C. Dohmen, T. Frohlich, U. Lachelt, I. Rohl, H. P. Vornlocher, P. Hadwiger, E. Wagner, *Mol. Ther. Nucleic Acids* **2012**, *1*, e7.

[48] R. Bonnett, *Chem. Soc. Rev.* **1995**, *24*, 19.

[49] I. J. MacDonald, T. J. Dougherty, *J. Porphyrins Phthalocyanines* **2001**, *5*, 105.

[50] C. Flors, M. J. Fryer, J. Waring, B. Reeder, U. Bechtold, P. M. Mullineaux, S. Nonell, M. T. Wilson, N. R. Baker, *J. Exp. Bot.* **2006**, *57*, 1725.

[51] A. Gollmer, J. Arnbjerg, F. H. Blaikie, B. W. Pedersen, T. Breitenbach, K. Daasbjerg, M. Glasius, P. R. Ogilby, *Photochem. Photobiol.* **2011**, *87*, 671.

[52] X. Ragas, A. Jimenez-Banzo, D. Sanchez-Garcia, X. Batllori, S. Nonell, *Chem. Commun.* **2009**, 2920.

[53] T. Lammers, P. Peschke, R. Kuehnlein, V. Subr, K. Ulbrich, P. Huber, W. Hennink, G. Storm, *Neoplasia* **2006**, *8*, 788.

[54] H. K. Moon, S. H. Lee, H. C. Choi, *ACS Nano* **2009**, *3*, 3707.